IEEE Transactions on Automation Science and Engineering (T-ASE) paper, presented at ICRA 2026, Vienna, Austria.
Cite as T-ASE paper.

Offline-Trained GAN-Augmented Highly Adaptive Control With Multi-DoF Fusion for Pneumatic Soft Surgical Robots

Yuxi Lu, *Member, IEEE*, Zhongchao Zhou, Dongliang Zheng, *Member, IEEE*, Yanmin Zhou, *Member, IEEE*, Zhipeng Wang, *Member, IEEE*, Shuo Jiang, *Member, IEEE*, Wenwei Yu, *Member, IEEE*, and Bin He, *Senior Member, IEEE*

***Abstract*—Pneumatic soft robots are well-suited for minimally invasive surgery owing to their compliance and safe interaction with tissues. However, achieving highly adaptive control is difficult owing to modeling inaccuracies, inter-chamber coupling, and disturbances from surgical instruments. Non-learning adaptive methods depend on simplified models and perform poorly in unstructured settings. Conversely, learning-based methods often impose high computational costs in multi-degree-of-freedom (multi-DoF) pneumatic systems. A previous study proposed a generative adversarial network (GAN)-based proportional–integral–derivative (G-PID) controller that combined PID stability with learning-based adaptability by aligning system behavior with a reference model. However, its performance in highly coupled multi-DoF pneumatic soft robots was unverified, and its online adversarial training was computationally intensive. We addressed these limitations by developing an offline-trained G-PID controller, shifting adversarial training offline to reduce computational overhead, achieving 23-fold faster convergence, and enabling real-time, model-free control with balanced adaptability and efficiency. We evaluated three multi-DoF data fusion strategies, showing effective coordination of DoF coupling while maintaining individual control fidelity. Validation on a multi-DoF soft robotic mechatronic system for single-port transvesical prostatectomy revealed tip errors below 0.16 mm across surgical instruments. Proposed controller enhances scalability and adaptability and may generalize to other mechatronic systems with nonlinear, coupled dynamics.**

***Note to Practitioners*—Pneumatic soft manipulators are attractive for minimally invasive procedures; however, they are difficult to control in practice: air chambers interact, simple models are inaccurate, and controllers that learn online can be too slow for real-time use. This work leverages a familiar PID loop and adds a compact compensator trained offline on short motion trials. In operation, the controller behaves like standard real-time system —no online learning or detailed physical model—while correcting for coupling and tool-induced disturbances. We also co mpared three multi-DoF fusion strategies and found that a unified fusion of all DoFs worked best. For a complete multi-DoF soft robotic mechatronic system designed for a single-port prostatectomy task, the approach maintained a tip error of less than 0.16 mm across different instruments, thereby reducing retuning effort and improving repeatability. Deployment involves collecting brief device-specific trajectories, training the compensator offline, and integrating it with existing pressure regulation and motion tracking. Current limitations include testing mainly planar motions on a four-chamber device, response speed constrained by pneumatic hardware, and the need for formal stability guarantees and automated tuning; higher-flow valves, revised chamber geometry, compact networks, and stability certification are practical next steps. Beyond surgery, the method is expected to transfer to other nonlinear, coupled mechatronic systems (e.g., continuum robots, pneumatic-muscle actuators, and compliant end-effectors).**

***Index Terms*—Adaptive control, generative adversarial network, manipulators, medical robotics, minimally invasive surgery, multi-DoF, soft robot, surgical robot.**

Received 19 September 2025; revised 10 November 2025; accepted 7 December 2025. Date of publication 16 December 2025; date of current version 12 January 2026. This article was recommended for publication by Associate Editor H. Wang and Editor L. Zhang upon evaluation of the reviewers' comments. This work was supported by the National Natural Science Foundation of China under Grant 62088101. *(Corresponding author: Zhongchao Zhou.)*

Yuxi Lu is with Shanghai Research Institute for Intelligent Autonomous Systems, the State Key Laboratory of Autonomous Intelligent Unmanned Systems, and the Frontiers Science Center for Intelligent Autonomous Systems of the Ministry of Education, Tongji University, Shanghai 201203, China, also with Shanghai Artificial Intelligence Laboratory, Shanghai 200232, China, and also with the Center for Frontier Medical Engineering, Chiba University, Chiba 263-8522, Japan (e-mail: yuxilu@tongji.edu.cn).

Zhongchao Zhou is with the School of Engineering, The University of Tokyo, Tokyo 113-0033, Japan (e-mail: zhouzhongchao@outlook.com).

Dongliang Zheng, Yanmin Zhou, Zhipeng Wang, Shuo Jiang, and Bin He are with Shanghai Research Institute for Intelligent Autonomous Systems, the State Key Laboratory of Autonomous Intelligent Unmanned Systems, and the Frontiers Science Center for Intelligent Autonomous Systems of the Ministry of Education, Tongji University, Shanghai 201203, China, and also with Shanghai Artificial Intelligence Laboratory, Shanghai 200232, China (e-mail: dzheng46@tongji.edu.cn; yanmin.zhou@tongji.edu.cn; wangzhipeng@tongji.edu.cn; jiangshuo@tongji.edu.cn; hebin@tongji.edu.cn).

Wenwei Yu is with the Center for Frontier Medical Engineering, Chiba University, Chiba 263-8522, Japan (e-mail: yuwill@faculty.chiba-u.jp).

This article has supplementary downloadable material available at https://doi.org/10.1109/TASE.2025.3644871, provided by the authors.

Digital Object Identifier 10.1109/TASE.2025.3644871

I. Introduction

PNEUMATIC soft robots—actuated by inflating multiple internal chambers—have emerged as promising flexible instruments for minimally invasive surgery owing to their inherent compliance and safe interaction with tissues [1], [2], [3]. Compared with conventional rigid laparoscopic instruments, these soft robotic devices can provide smoother navigation through convoluted anatomical pathways and transmit considerably lower contact forces [4], thereby reducing the risk of iatrogenic injury. Recent demonstrations—including soft robotic manipulators for precise laser positioning, steerable colonoscopes, and variable-stiffness endoluminal arms—have highlighted their superior dexterity and enhanced safety compared with conventional rigid instruments [5], [6], [7].

Nevertheless, achieving accurate and multistep surgical maneuvers using pneumatic soft robots remains a major

IEEE Transactions on Automation Science and Engineering (T-ASE) paper, presented at ICRA 2026, Vienna, Austria.

challenge. Controlling multi-degree-of-freedom (multi-DoF) pneumatic soft robots requires the simultaneous pressurization of several chambers. This pressurization induces considerable geometric coupling, wherein the deformation of one chamber restricts or modifies that of another [8]. Such interactions undermine dynamic models and hinder real-time trajectory tracking within the ± 1 mm accuracy clinical threshold.

Moreover, the low stiffness of pneumatic soft robots can complicate control when instruments such as 5–8 mm flexible endoscopes or fiber-optic catheters are inserted through their internal channels. Instrument insertion introduces friction, compression, and stochastic micro-slips [9], [10]. As clinical endoscopes vary widely in diameter, curvature, and internal mechanics, a single deterministic model cannot capture all instrument–robot interactions. Consequently, controllers must be capable of handling the intrinsic nonlinear coupling within soft robots and external disturbances introduced by unknown surgical instruments to ensure safe and accurate motion. Several methods have been proposed to tackle the challenge of adaptability in control systems. These can generally be categorized into learning- and non-learning-based methods.

A. Non-Learning-Based Adaptive Control Strategies

In conventional control theory, several non-learning-based controllers have been developed to address uncertainty and model inaccuracy [11], [12], [13]. Among them, robust controllers such as the H∞ and sliding-mode controllers are widely used [14], [15]. Although these methods are not adaptive controllers in the strict sense, their robustness enables them to effectively handle unknown variations, thereby achieving a form of implicit adaptability. Other methods aim to adapt to system changes by dynamically tuning the control gains or identifying unknown system parameters in real time. These methods fall within the classical adaptive control framework, which includes direct and indirect adaptive controllers [16]. Such methods have been widely applied in the field of soft robots. For example, Best et al. [17] applied a nonlinear model predictive control strategy to a multi-chamber pneumatic arm, which is a typical example of indirect adaptive control, and achieved submillimeter accuracy.

Although some strategies involve dynamic adjustment, non-learning-based adaptive control strategies do not rely on large-scale data or neural network-based training; hence, they are classified as non-learning methods [18]. A primary limitation of these methods is their strong dependence on an accurate dynamic model, as most are inherently model-based [19], [21],. Moreover, the absence of network-based updates implies that tuning adaptation rules and related parameters can be complex and nontrivial.

B. Learning-Based Adaptive Control Strategies

Another class of adaptive controllers—referred to as learning-based adaptive control—leverages neural networks and large-scale data [22]. Recent advances in data-driven control have further broadened this paradigm, particularly in precision automation and microrobotics. For instance, Zhong et al. [23] proposed a disturbance rejection framework for paired magnetic millirobots in confined spaces, achieving highly accurate motion control through data-driven disturbance compensation under global inputs. Similarly, Wang et al. [24] developed a parallel adaptive control scheme for magnetic helical microrobots in uncertain environments, achieving robust real-time performance by incorporating derivative structures into the learning loop. Although these methods differ from classical adaptive control in terms of their implementation, they share common mechanisms for achieving adaptability, such as adjusting the control gains or performing online system identification. A typical example is using neural networks to fine-tune the control gains of a feedback controller, which could be model- or error-based—for example, a proportional–integral–derivative (PID) controller [25]. In addition, deep reinforcement learning can achieve adaptability and generalization by allowing agents to learn control policies through extensive interactions with the environment [26], [27], [29],. This class of methods has gained considerable traction in soft robot control applications. For example, Centurelli et al. [26] employed trust-region policy optimization for payload-robust trajectory tracking.

Despite their potential, learning-based adaptive control strategies typically require extensive datasets and prolonged online training, often involving tens of thousands of interactions and training times of several minutes. This level of inefficiency is impractical in real-time surgical applications. Moreover, the theoretical guarantees for learning-based adaptive controllers regarding stability and robustness remain limited, particularly in the presence of sudden disturbances. Most importantly, consistent control performance cannot be assured, particularly in safety-critical tasks such as surgical manipulation [30].

Motivated by the complementary, yet incomplete, advantages of non-learning- and learning-based control paradigms, Zhou et al. [31] proposed a generative adversarial network (GAN)-based PID (G-PID) architecture to achieve high adaptability. The G-PID controller combined classical PID control stability with learning-based adaptability. The device comprised a generator that produced compensation actions to enhance PID responsiveness when controlling an unknown/changing system. Moreover, a discriminator was essential for achieving highly adaptive control because it continually distinguished responses from the compensated unknown or changing system and the predefined reference system. By consistently updating the compensator based on this discrimination, the system could dynamically align the response of the unknown system with that of the reference system, thereby realizing robust adaptive control. Without this discriminator-driven adversarial learning mechanism, real-time adaptability could not be achieved.

Online-trained G-PID requires updates at each time step, which incurs considerable computational costs. In addition, soft robotic systems typically exhibit strong nonlinearities, particularly in multi-DoF scenarios. The coupling of different joints or actuators can lead to large variations in the gradient across time steps. As the online-trained G-PID relies on a single-step update, it is particularly sensitive to abrupt gradient changes, potentially resulting in instability or suboptimal control performance.

IEEE Transactions on Automation Science and Engineering (T-ASE) paper, presented at ICRA 2026, Vienna, Austria.

In this study, an offline-trained G-PID controller specifically tailored to multi-DoF soft robots was introduced to overcome these limitations. By shifting the adversarial training process offline, the computational demand could be reduced considerably, resulting in 23-fold faster convergence and enabling stable and safe hyperparameter tuning. In addition, three distinct multi-DoF fusion strategies were proposed and evaluated to efficiently convey the inter-chamber coupling characteristics to the generator network.

The proposed controller was validated on a four-chamber pneumatic soft robot designed for single-port transvesical prostatectomy via simulations and physical experiments. The results revealed that the offline-trained G-PID consistently achieved tip position errors below 0.9 mm relative to the reference response under varying surgical instrument and payload conditions. The controller closely replicated the transient dynamics of the reference model, meeting the stringent accuracy requirements for minimally invasive surgical procedures.

The main contributions of this study are as follows:

1) **Offline-Trained G-PID Architecture** An offline adversarially trained compensator achieved approximately 23 times faster convergence and improved closed-loop stability compared with an online baseline.
2) **Multi-DoF Data Fusion Strategies** We systematically compared three multi-DoF data fusion strategies—that is, batch-separated DoF conditioning, independent DoF modularization, and unified DoF modularization—to identify how the generator network could effectively handle complex inter-DoF coupling while preserving individual DoF-specific characteristics. This comparative study revealed optimal fusion strategies that could enhance the adaptability and robustness of controllers in multi-DoF pneumatic soft robots.
3) **Comprehensive Experimental Validation** Extensive hardware and simulation tests on a four-chamber soft manipulator designed for single-port prostatectomy demonstrated high adaptability across surgical instruments, effective compensation for coupling effects and tool interactions, and accurate adherence to the reference model response. The proposed controller, validated through soft surgical robotic applications, enhances scalability and adaptability and is expected to be generalizable to other mechatronic systems with nonlinear and coupled dynamics.

II. Proposed Controller Design and Multi-DoF Fusion

A. Offline-Trained G-PID Controller

The proposed offline-trained G-PID controller for soft robots is illustrated in Fig. 1. Unlike the online-trained G-PID method presented by Zhou et al. [31], which requires gradient updates at every discrete control interval, the offline-trained G-PID controller separates the training process into two distinct phases—that is, real-time control and offline update.

As shown in Fig. 1a, during the control phase, no updates are performed; thus, the discriminator remains completely inactive, whereas the generator functions entirely as a lead

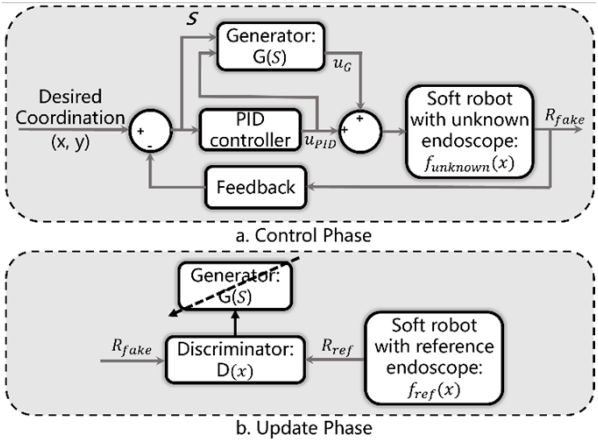

Fig. 1. Flowchart of the offline-trained G-PID controller.

compensator. Data from the reference system are not required during this phase. The generator network $G(s)$ receives the real-time system state information S and produces an adaptive compensation signal u_G. This compensatory signal is combined with the PID output u_{PID} and applied to the pneumatic soft robot that is inserted with an unknown endoscope, represented by $f_{unknown}(x)$. The response of the unknown system $f_{unknown}(x)$ is termed the fake response R_{fake}.

A fake response is recorded throughout the control phase without immediate parameter updates, thereby ensuring stable real-time operation.

In the subsequent offline update phase, $f_{unknown}(x)$ does not participate because the system does not involve a control process. Only the recorded R_{fake} from the control phase is required. Owing to this characteristic, this method is referred to as the offline-trained G-PID controller. The recorded fake response R_{fake} and predefined reference response R_{ref}, generated by the soft robot equipped with a known reference endoscope, are simultaneously provided to the discriminator $D(x)$. The discriminator receives these responses and guides the adversarial updates of the generator to optimize its compensation capability. Both networks are trained offline based on the adversarial loss function $V(G, D)$ defined as follows:

$$\min_G \max_D V(G,D) = \mathbb{E}_{R_{ref}\sim p_{data}(R_{ref})}\left[logD\left(R_{ref}\right)\right] + \mathbb{E}_{fake\sim p_{data}(R_{fake})}[\log\left(1-R_{fake}\right)] \quad (1)$$

Here, $R_{ref} \sim p_{data(R_{ref})}$ are reference-response samples generated by the reference model, and $fake \sim p_{data(R_{fake})}$ are compensated responses produced by the generator G. The discriminator D outputs the probability that an input originates from p_{ref}. The first expectation encourages the correct classification of reference responses, whereas the second penalizes assigning high reference probability to generated responses; the resulting min–max optimization drives p_G toward p_{ref}, making the compensated closed-loop response indistinguishable from the reference and thereby improving adaptability.

Detailed pseudocode outlining the offline-trained G-PID training and implementation procedures is presented in Table I. Unless otherwise noted, all models were trained with identical

IEEE Transactions on Automation Science and Engineering (T-ASE) paper, presented at ICRA 2026, Vienna, Austria.

TABLE I
PSEUDOCODE OF THE OFFLINE-TRAINED G-PID CONTROLLER

Algorithm 1 Offline GAN-based PID controller

Initialize G, D; select a reference system

Run the reference system and record all state information as a reference response

1. **For epochs** → max epochs **do**
2. **For** T → max control time **do**
3. Run control period and record all state information as a fake response
4. **END For**
5. **For** iterations à max iterations do (**Train D**)
6. Update the discriminator on all reference and fake data
7. **End For**
8. **For** iterations à max iterations do (**Train G**)
9. Update the generator on all reference and fake data
10. **End For**
11. **End All**

hyperparameters to isolate the effects of the training strategy and fusion mechanisms. The learning rates for the generator and discriminator were fixed at (2×10^{-4}); training was run for 500 epochs with a batch size of 1. No explicit regularization or early stopping was applied, and the final-epoch weights were used for evaluation.

B. Proposed Multi-DoF Fusion

We systematically explored the effective integration of multi-DoF information within the proposed offline-trained G-PID controller by introducing and comparing three fusion strategies—batch-separated DoF conditioning, independent DoF modularization, and unified DoF modularization—selected to span a clear spectrum from minimal to full information sharing, thereby enabling a structured assessment of how inter-DoF coupling should be exploited in coupled pneumatic multi-DoF systems. The fusion strategies are described as follows:

1) Batch-Separated DoF Conditioning(Fig. 2a): For this strategy, the input data corresponding to each DoF are separated into distinct batches, with clear DoF-specific identifiers (one-hot embedding-style conditioning signals) integrated into each batch. Although processed independently within batches, all data are evaluated using the same generator and discriminator. The generator and discriminator implicitly maintain the awareness of the DoF distinctions via DoF-specific identifiers, thereby facilitating the efficient handling of the interactions between coupled DoFs.

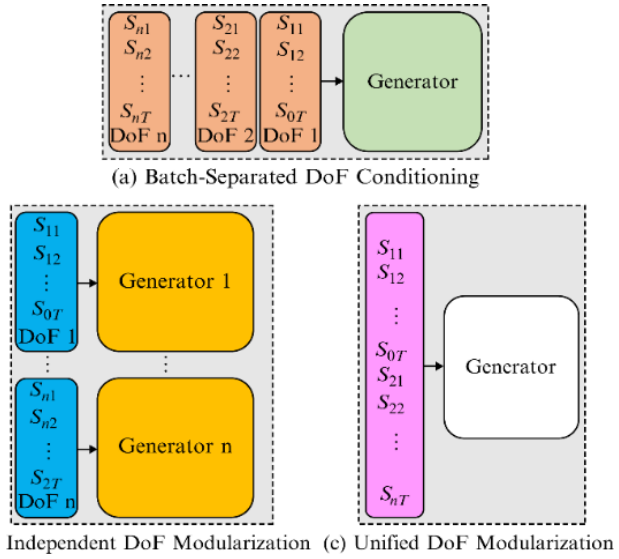

Fig. 2. Three multi-DoF training fusions.

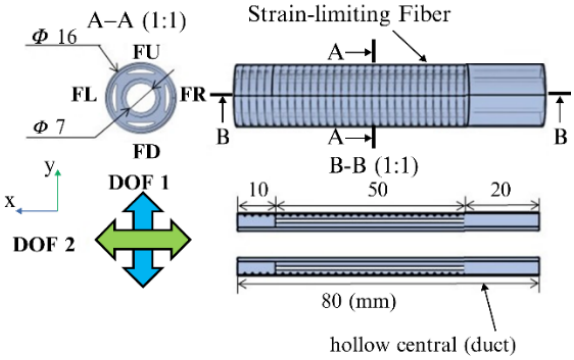

Fig. 3. Structure of soft robots.

2) Independent DoF Modularization(Fig. 2b): This strategy employs independent generator–discriminator modules for each DoF. Such modularization permits the independent processing and assessment of specific dynamics for each DoF, enhancing the capability of the generator to distinctly learn and compensate for individual chamber behaviors.

3) Unified DoF Modularization (Fig. 2c): The unified DoF modularization strategy concatenates information from all DoFs into a single unified input vector, which is fed into the discriminator and generator networks. Consequently, the input and output dimensionalities of the generator scale proportionally with the total number of DoFs, enabling the network to directly capture the interactions among the DoFs. The discriminator is also provided with these integrated DoF configurations, thereby enabling the coupling characteristics to be modeled in a unified manner.

III. EXPERIMENTAL METHODS

A. Soft Robot Modeling

Fig. 3 illustrates the design and structural details of a soft robot specifically designed for endoscopic surgery applications featuring two DoFs.

IEEE Transactions on Automation Science and Engineering (T-ASE) paper, presented at ICRA 2026, Vienna, Austria.

These DoFs are actuated by four symmetrically arranged pneumatic chambers—that is, the FU, FD, FL, and FR chambers. The two orthogonally oriented DoFs collectively enable critical surgical tasks, such as precise prostate probing, suturing, and tissue dissection. A hollow central channel (duct) was designed to accommodate endoscopes with diameters up to 6 mm. In this study, a soft robot was fabricated from silicone rubber (SIL30, San Draw Inc., TWN) using 3D silicon printing (S053 Silicone 3D Printer, San Draw Inc., TWN).

Accurately establishing a dynamic model remains challenging owing to the complex interactions between the soft robot and the inserted endoscopes, as well as the inherently nonlinear material properties and pneumatic behavior of the soft robot.

We addressed these complexities by adopting a modeling approach inspired by previous studies [32], [33], [34], approximating the robot dynamics as a superposition of two overdamped second-order systems. The simplified system response model can be expressed as follows:

$$x(t) = C_1 e^{-\lambda_1 t} + C_2 e^{-\lambda_2 t} + C_3 \tag{2}$$

where $x(t)$ denotes the tip position of the robot, and C_1, C_2, and C_3 denote the amplitude coefficients dependent on the initial conditions and input pressures. In particular, C_3 denotes the steady-state displacement and must remain positive; λ_1 and λ_2 denote positive decay rates.

According to a previous study [30], each distinct input pressure step yields a unique dynamic response. Thus, discrete step pressure inputs were applied to the robot, and their corresponding transient responses were recorded. Subsequently, the parameters λ_1, λ_2, C_1, C_2, and C_3 were identified via the least-squares method to best fit the experimentally obtained step responses.

As these parameters varied with the input pressure, each parameter was further modeled using polynomial regression with respect to two pressure inputs: p_1 (pressure applied to the chambers FL and FR) and p_2 (pressure applied to the chambers FU and FD). Their polynomial forms can be expressed as follows:

$$\lambda_1(\mathrm{p}_1, p_2) = \sum_{i=0}^{m} \sum_{j=0}^{m-i} a_{ij} p_1^i p_2^j \tag{3}$$

$$C_1(\mathrm{p}_1, p_2) = \sum_{i=0}^{m} \sum_{j=0}^{m-i} b_{ij} p_1^i p_2^j \tag{4}$$

where a_{ij} and b_{ij} denote regression coefficients determined through the least-squares fitting procedure, and m denotes the polynomial degree selected based on the optimal balance between model accuracy and complexity. As λ_1, C_2, and C_3 share the same form, their expressions are omitted.

The simulations and experiments were conducted in discrete time. As such, (2) was discretized using the backward Euler method. In particular, it was decomposed into three separate terms, as follows:

$$x(t) = x_1(t) + x_2(t) + x_3(t) \tag{5}$$

where $x_1(t) = C_1 e^{-\lambda_1 t}$, $x_2(t) = C_2 e^{-\lambda_2 t}$, and $x_3(t) = C_3$. Taking the time derivative of $x_1(t)$ yields

$$\frac{dx_1(t)}{dt} = -\lambda_1 x_1(t) \tag{6}$$

Applying the backward Euler discretization to (6),

$$\frac{dx_1(t)}{dt}\Big|_{t=n\Delta t} \approx \frac{x_1(n) - x_1(n-1)}{\Delta t} = -\lambda_1 x_1(n) \tag{7}$$

Rearranging the terms, the discrete form for $x_1(n)$ is

$$x_1(n) = \frac{x_1(n-1)}{1 + \lambda_1 \Delta t} \tag{8}$$

Similarly, the discrete form for $x_2(n)$ can be obtained as

$$x_2(n) = \frac{x_2(n-1)}{1 + \lambda_2 \Delta t} \tag{9}$$

Considering $x_3(n)\, \mathrm{x}_3\,(\mathrm{n})$ as a constant steady-state term, the final discrete form of (2) is

$$x(n) = \frac{x_1(n-1)}{1 + \lambda_1 \Delta t} + \frac{x_2(n-1)}{1 + \lambda_2 \Delta t} + C_3 \tag{10}$$

where n denotes the time step, and Δt denotes the discretization time step.

B. Prototype Experiment Setting for Soft Robot Modeling

The dynamic response of the robot was experimentally characterized by sequentially applying discrete step pressures (10, 20, 30, …, 180 kPa). Owing to the symmetrical geometry and material uniformity of the robot, two representative chamber combinations were measured—that is, a single-chamber (FL) and a two-chamber combination (FL and FU). This was sufficient to fully characterize the dynamic response of all four chambers, thereby simplifying the experimental procedure and avoiding redundancy. Each pressure step was maintained for 10 s to ensure stable response data collection. The responses for the symmetric chambers (FR and FD) were inferred directly from the recorded responses of the FL and FU chambers.

An Arduino Uno Rev3 microcontroller (Arduino CC, USA) served as the main control unit and regulated the air pressure through a proportional valve (SMC ITV0050-2ML, SMC Co., Ltd., Japan). A high-precision pressure sensor (KP201, Shenzhen Dahua Electronics Co., Ltd., CN, accuracy ±1 kPa) was used to record the applied air pressures. In addition, a motion tracking system (Mars 4H, Beijing NOKOV Science & Technology Co., Ltd., CN) tracked the robot tip position during each 10 s interval. A reflective marker was affixed to the tip of the robot to enhance the positional tracking accuracy.

The positional data collected at each pressure step were analyzed using the previously defined response model ((3) and (4)). Step-response measurements were systematically performed under two conditions—that is, without an endoscope and with endoscopes of different diameters inserted into the central channel of the robot. The endoscopes used in this study were the Ambu® aScope 4 Broncho Slim (3.8 mm diameter), Ambu® aScope 4 Broncho Regular (5.0 mm diameter), and Ambu® aScope 4 Broncho Cysto (5.4 mm diameter).

C. Simulation Experiment Setting for the Offline-Trained G-PID Controller

Fig. 4 illustrates the architectures of the generator and discriminator employed in this study. All input signals were

IEEE Transactions on Automation Science and Engineering (T-ASE) paper, presented at ICRA 2026, Vienna, Austria.

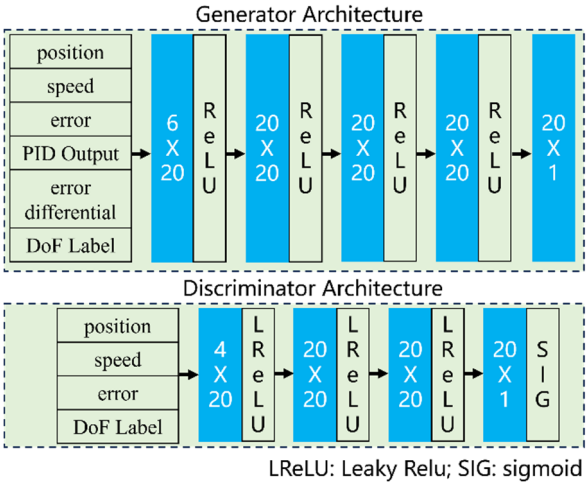

Fig. 4. Network architecture.

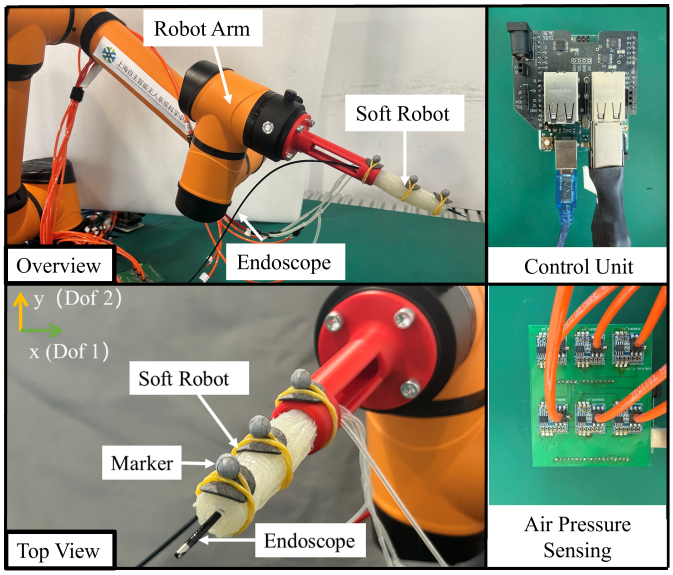

Fig. 5. Prototype experiment setting.

used in their native physical units (i.e., without normalization or standardization) to preserve the physical correspondence and relative magnitudes between the state, error, and control variables, thereby maintaining closed-loop interpretability. This design choice avoids confounding architectural effects in the offline–online and multi-DoF fusion comparisons and is consistent with prior G-PID analyses [31]. The generator receives the system state information S as the input (Fig. 1a), including the robot's tip position, velocity, position tracking error, PID output, and derivative of the tracking error, and outputs a compensation signal u_G. Conversely, the discriminator receives the robot's tip position, velocity, and position tracking error as inputs. Both networks are implemented as multilayer perceptrons (MLPs). The generator comprises five layers using rectified linear unit (ReLU) activations in the hidden layers, whereas the discriminator comprises four layers with LeakyReLU (LReLU) activations and a sigmoid output layer. The network architectures and input–output features follow the designs proposed in [31], which have demonstrated stable and effective performance in control-compensation tasks.

Static MLPs were deliberately adopted instead of time-aware architectures (e.g., RNNs or LSTMs) to maintain the study's focus on comparing offline and online training strategies and different multi-DoF fusion mechanisms, without introducing architectural biases. Moreover, recurrent or sequence-based models typically incur greater computational overhead and inference latency, which would hinder real-time execution on embedded hardware. The MLP structure thus provides a balanced trade-off between representational capability, computational efficiency, and reproducibility, making it more suitable for real-time adaptive control experiments.

The reference system response (R_{ref}, as illustrated in Fig. 1b) was modeled based on a soft robot without an endoscope because this scenario provided the fastest response among the tested configurations. Conversely, the response model of the robot with a 5.4-mm diameter endoscope inserted was selected as the unknown system during GAN training. This selection follows model reference adaptive control (MRAC) practice [35]: a realizable, fast, low-overshoot reference was used. Comparable performance held for similar-bandwidth references; overly aggressive ones exceeded hardware limits and degraded tracking. Additional validations were performed using endoscopes with diameters of 3.8 and 5.0 mm inserted into the soft robot.

For the PID controller parameters, DoFs 1 and 2 were set to the same gains ($k_p = 10$, $k_i = 15$, and $k_d = 5$) with a discretized control timestep of 0.02 s and a total control period of 10 s. The offline-trained G-PID controller was trained by training all three multi-DoF fusions over 400 epochs.

The benchmark for the effectiveness of the proposed offline training approach was set by training an online-trained G-PID controller using a batch-separated DoF conditioning strategy for direct comparative evaluation. The Adam optimizer, with a learning rate of $2e^{-4}$, was employed to optimize both the generator and discriminator parameters. All neural network models were developed in Python 3.9.12 (64-bit) using PyTorch version 1.12.1 and CUDA 11.3 acceleration.

D. Prototype Experiment Setting for the Offline-Trained G-PID Controller

Fig. 5 illustrates the complete multi-DoF soft robotic mechatronic system employed for real-world validation of the offline-trained G-PID controller. The system configuration, including the control unit, pressure regulation mechanisms, and motion tracking unit, remained consistent with the setup previously described in Section III-B.

In the prototype validation experiments, an offline-trained G-PID controller initially trained in the simulation was directly deployed for soft robot control in real-world conditions. A revised set of PID gains ($k_p = 25$, $k_i = 92$, and $k_d = 1$) was determined empirically by tuning to address discrepancies commonly encountered during sim-to-real transfers. These revised gains ensured that the robot's response without the inserted endoscope closely matched the reference response defined in the simulation.

IEEE Transactions on Automation Science and Engineering (T-ASE) paper, presented at ICRA 2026, Vienna, Austria.

TABLE II
MSE FOR EACH FITTING GROUP

Endoscope diameter	Without	3.8 mm	5.0 mm	5.4 mm
MSE (mm^2)	0.77	0.07	0.39	0.09

Additional validation tests were performed using medical-grade endoscopes, which differ distinctly from those employed in the simulation-based robot-modeling experiments (Section III-B) to further evaluate the adaptability and generalization capability of the proposed controller to realistic clinical conditions. In particular, clinical endoscopes from Innovex Medical Co., Ltd. (CN) were selected. These included a single-use flexible ureterorenoscope (2.7 mm), a single-use flexible bronchoscope (4.2 mm), and a single-use flexible cystoscope (5.5 mm).

IV. RESULTS

A. Response Model Fitting Results

During the parameter fitting of the amplitude coefficients (C_1, C_2, C_3) and decay rates (λ_1, λ_2) using (3) and (4), we observed that coefficients C_1 and C_2, as well as decay rates λ_1 and λ_2, consistently converged to identical values. This symmetry arose from the inherent geometric symmetry of the actuator and uniform chamber response characteristics, enabling the original model ((2)) to be simplified into the following first-order form:

$$x(t) = 2C_1 e^{-\lambda_1 t} + C_3 \tag{11}$$

The regression coefficients from the polynomial fitting are detailed in the Appendix. A quantitative evaluation, conducted through a mean squared error (MSE) comparison between the measured responses and the predictions from the simplified model, demonstrated comparable accuracy (summarized in Table II), thereby confirming the practical validity of the model.

The simplification to a first-order model is consistent with the observed slow response of the actuator and absence of an overshoot. These dynamic characteristics could be attributed primarily to the small chamber volume and hollow central duct of the actuator. Initially, the limited chamber volume restricted rapid deformation upon pressurization. Subsequently, the central duct inflated inward, delaying notable curvature and effectively reducing the dynamic complexity. Such response behavior is consistent with the finite element analyses in previous literature [36], which similarly reported delayed bending owing to inward inflation in hollow actuators, further supporting our simplified first-order representation as physically meaningful and practically sufficient for adaptive control purposes.

Unified DoF modularization demonstrated superior compensation in DoF 1, which closely matched the reference trajectory. However, its performance in DoF 2 exhibited noticeable overcompensation, suggesting that although the transient response stability and settling time were improved relative to the PID-only control, further parameter refinement or strategy optimization may be necessary to achieve precise alignment with the reference system.

We evaluated the effectiveness of the offline and online-trained G-PID controllers [31] in multi-DoF pneumatic soft robotic systems by conducting a comparative study under the unified DoF modularization framework using identical experimental conditions. As shown in Figs. 6a and b, the online-trained G-PID controller exhibited limited compensation capability under the optimal multifusion strategies, producing a response that closely resembled that of the PID-only controller. By contrast, the offline-trained G-PID controller achieved notably improved tracking accuracy and stability.

TABLE III
AVERAGE TRAINING DURATION FOR EACH CONFIGURATION

	Unified	Batch	Independent	Online
Time	954 s	1093 s	1045 s	22281 s

TABLE IV
SYSTEM TIME RESPONSE CHARACTERISTICS UNDER THE OFFLINE-TRAINEDG-PID (VS. PID) CONTROLLER

DoF 1	5.0 mm	3.8 mm	Reference
Settling time	4.74 s (5.48 s)	4.76 s (6.96 s)	4.02 s
Delay time	1.28 s (2.34 s)	1.10 s (2.12 s)	1.54 s
Rising time	3.74 s (6.78 s)	3.74 s (5.56 s)	3.40 s

DoF 2	5.0 mm	3.8 mm	Reference
Settling time	4.34 s (5.76 s)	4.32 s (5.80 s)	3.76 s
Delay time	1.04 s (1.60 s)	0.92 s (1.40 s)	0.86 s
Rising time	2.28 s (4.78 s)	2.16 s (3.10 s)	2.04 s

B. Offline-Trained G-PID Controller in Simulation Experiment

First, the training durations of the offline and online-trained G-PID controllers were compared. The online-trained G-PID used a unified DoF modularization strategy to transmit DoF information. In addition, the training durations for all three multi-DoF fusion strategies were assessed for the offline-trained G-PID controller. Each configuration was independently trained three times, the average training durations of which are summarized in Table III. The results clearly demonstrate that offline training substantially improved the computational efficiency, reducing the training time 23-fold compared with online training. Variations among the multi-DoF fusions exhibited a negligible impact on the offline training duration.

We evaluated the adaptability of the offline-trained G-PID controller by testing it on soft robots with 5.0- and 3.8-mm endoscopes. Table IV summarizes the performance metrics of these systems. Under PID control alone, the settling time difference between the 3.8 mm system and the reference system was approximately 2.94 (6.96−4.02) s; employing offline-trained G-PID control reduced this discrepancy con-

IEEE Transactions on Automation Science and Engineering (T-ASE) paper, presented at ICRA 2026, Vienna, Austria.

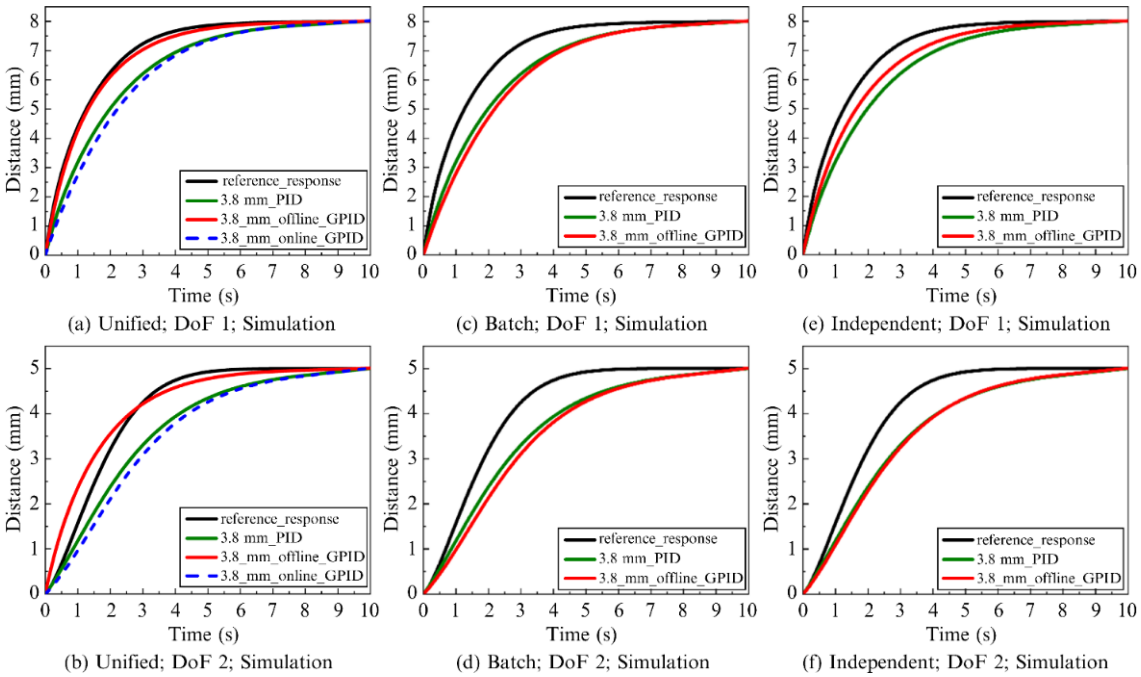

Fig. 6. Comparison of the responses for the three DoF information fusion strategies. a) Unified DoF modularization, DoF 1; b) Unified DoF modularization, DoF 2; c) Batch-separated DoF conditioning, DoF 1; d) Batch-separated DoF conditioning, DoF 2; e) Independent DoF modularization, DoF 1; f) Independent DoF modularization, DoF 2.

siderably, to 0.74 (4.76−4.02) s. Similarly, the initial settling time difference of 1.48 s between the 3.8- and 5.0-mm systems decreased to just 0.02 (4.76−4.74) s with offline-trained G-PID control. Moreover, notable reductions in the delay and rising times were evident across both DoFs, further validating the adaptability of the offline-trained G-PID controller.

Fig. 6 compares three different multi-DoF fusion strategies for training the offline-trained G-PID controller. The results indicate that the unified DoF modularization consistently delivered the most accurate compensatory performance across both DoFs. Conversely, batch-separated DoF conditioning, employed in [31], exhibited poor performance, producing compensation signals in directions opposite to that of the required action. Independent DoF modularization demonstrated limited effectiveness, providing moderate compensation in DoF 1 but failing entirely in DoF 2, indicating its constrained adaptability to multi-DoF scenarios.

Unified DoF modularization demonstrated superior compensation in DoF 1, which closely matched the reference trajectory. However, its performance in DoF 2 exhibited noticeable overcompensation, suggesting that although the transient response stability and settling time were improved relative to the PID-only control, further parameter refinement or strategy optimization could be necessary to achieve precise alignment with the reference system.

We evaluated the effectiveness of the offline and online G-PID controllers [31] in multi-DoF pneumatic soft robotic systems by conducting a comparative study under the unified DoF modularization framework using identical experimental conditions. As shown in Figs. 6a and b, the online G-PID controller exhibited limited compensation capability under the optimal multifusion strategies, producing a response that closely resembled that of the PID-only controller. By contrast, the offline-trained G-PID controller achieved notably improved tracking accuracy and stability.

C. Offline-Trained G-PID Controller in the Prototype Experiment

Fig. 7 presents the prototype validation results for the offline-trained G-PID controller using three clinically relevant endoscopes (2.7, 4.2, and 5.5 mm), which differed from those used in simulation training. For all three tested endoscopes, the offline-trained G-PID controller successfully compensated for the discrepancies evident under PID-only control, maintaining the actuator tip trajectories consistently close to the predefined reference response. In particular, at each discrete control timestep, the maximum deviation between the actual response under offline-trained G-PID control and the reference response remained below ±0.9 mm. By contrast, the PID-only control consistently exhibited maximum deviations greater than ±1.5 mm.

Table V summarizes the maximum and average deviations for each controller-endoscope combination. Under PID-only control, the maximum errors were consistently larger than ±1 mm, with average errors exceeding ±0.5 mm. Conversely, the offline-trained G-PID controller reduced these deviations considerably, maintaining maximum errors below ±0.9 mm and average errors below ±0.2 mm.

V. Discussion

A. Offline-Trained G-PID Controller in the Simulation Experiment

Several advantages of the proposed offline-trained G-PID controller were verified. Table IV demonstrates the improvements in the training efficiency achieved with offline

IEEE Transactions on Automation Science and Engineering (T-ASE) paper, presented at ICRA 2026, Vienna, Austria.

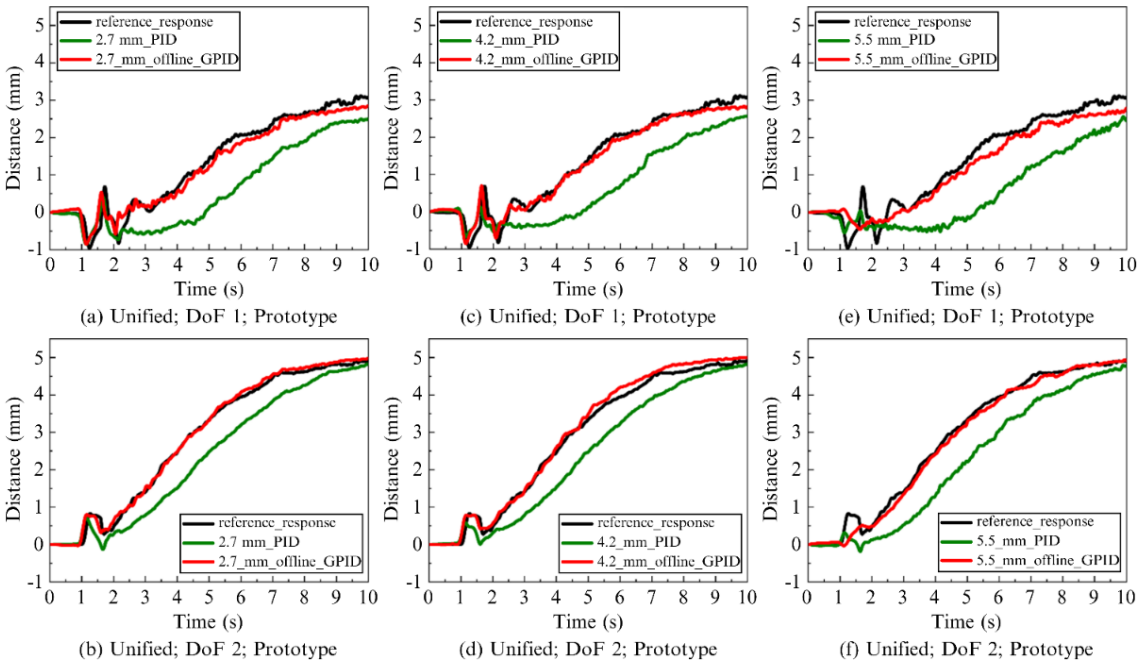

Fig. 7. Experimental validation results of the offline G-PID controller performance across different clinical endoscopes. (a) Single-use flexible ureterorenoscope (2.7 mm), DoF 1; (b) Single-use flexible ureterorenoscope (2.7 mm), DoF 2; (c) Single-use flexible bronchoscope (4.2 mm), DoF 1; (d) Single-use flexible bronchoscope (4.2 mm), DoF 2; (e) Single-use flexible cystoscope (5.5 mm), DoF 1; (f) Single-use flexible cystoscope (5.5 mm), DoF 2.

TABLE V

MAX AND AVERAGE ERROR OF THE OFFLINE-TRAINED G-PID(VS. PID) CONTROLLER

DoF 1	2.7 mm	4.2 mm	5.5 mm
Max	0.86 mm (1.54 mm)	0.89 mm (1.52 mm)	0.68 mm (1.89 mm)
Average	0.16 mm (0.81 mm)	0.13 mm (0.79 mm)	0.20 mm (0.96 mm)

DoF 2	2.7 mm	4.2 mm	5.5 mm
Max	0.21 mm (1.09 mm)	0.28 mm (1.08 mm)	0.69 mm (1.27 mm)
Average	0.07 mm (0.55 mm)	0.12 mm (0.52 mm)	0.10 mm (0.71 mm)

TABLE VI

REGRESSION COEFFICIENTS FOR λ_1

λ_1	Without [*1]	3.8 mm[*2]	5 mm	5.4 mm
p_1	$3.9e^{-5}$	$7.14e^{-5}$	$-2.14e^{-4}$	$7.01e^{-5}$
p_2	$-1.12e^{-3}$	$8.6e^{-4}$	$9.9e^{-4}$	$3.55e^{-3}$
p_1^2	$-1.96e^{-5}$	$-1.80e^{-5}$	$-3.42e^{-6}$	$-2.36e^{-5}$
p_2^2	$-4.63e^{-5}$	$-1.94e^{-5}$	$-6.05e^{-6}$	$-3.29e^{-5}$
Bias	1.23	1.15	1.03	1.41

[*1] Without an endoscope inserted, the regression coefficients associated with λ_1; [*2] With a 3.8 mm endoscope inserted, the regression coefficients associated with λ_1.

TABLE VII

REGRESSION COEFFICIENTS FOR C_1

C_1	Without[*3]	3.8 mm	5.0 mm	5.4 mm
p_1	-0.0224	$1.44e^{-2}$	$1.06e^{-2}$	0.0176
p_2	$1.1e^{-4}$	$-2.28e^{-3}$	$-1.02e^{-2}$	$-2.16e^{-3}$
p_1^2	$4.41e^{-6}$	$5.34e^{-7}$	$9.66e^{-6}$	$-6.71e^{-7}$
p_2^2	$-4.32e^{-18}$	$-5.00e^{-17}$	$2.04e^{-16}$	$6.38e^{-17}$
p_1p_2	$-2.45e^{-4}$	$-1.36e^{-4}$	$-9.01e^{-5}$	$-1.82e^{-4}$
p_1^3	$6.73e^{-6}$	$1.73e^{-6}$	$1.57e^{-6}$	$9.37e^{-7}$
p_2^3	$1.01e^{-6}$	$7.10e^{-7}$	$6.87e^{-7}$	$1.28e^{-6}$
Bias	-0.163	-0.0653	-0.119	0.0388

[*3] All definitions are identical to those in *1.

TABLE VIII

REGRESSION COEFFICIENTS FOR C_3

C_3	Without	3.8 mm	5.0 mm	5.4 mm
p_1	$2.24e^{-2}$	$1.44e^{-2}$	$1.06e^{-2}$	0.0176
p_2	$1.10e^{-4}$	$-2.28e^{-3}$	$-1.02e^{-2}$	$-2.16e^{-3}$
p_1^2	$4.41e^{-6}$	$5.34e^{-7}$	$9.66e^{-6}$	$-6.71e^{-7}$
p_2^2	$-4.32e^{-18}$	$-5.00e^{-17}$	$2.04e^{-16}$	$6.38e^{-17}$
p_1p_2	$-2.45e^{-4}$	$-1.36e^{-4}$	$-9.01e^{-5}$	$-1.82e^{-4}$
p_1^3	$6.73e^{-6}$	$1.73e^{-6}$	$1.57e^{-6}$	$9.37e^{-7}$
p_2^3	$1.10e^{-6}$	$7.10e^{-7}$	$6.87e^{-7}$	$1.28e^{-6}$
bias	-0.163	-0.0653	-0.119	0.0388

training, particularly as the DoFs and data volume of the system increased. In addition, offline training optimized compensatory actions considering the entire system trajectory, whereas online training updated the parameters at each time step, risking convergence to the local minimum, which is beneficial only over limited intervals. Nevertheless, the online method retained the unique advantage of dynamically adapting to exceptionally irregular response behaviors, which is a capability absent in offline methods.

IEEE Transactions on Automation Science and Engineering (T-ASE) paper, presented at ICRA 2026, Vienna, Austria.

Moreover, offline training enhanced numerical stability by mitigating the adverse effects of the large gradient fluctuations frequently encountered during online training. However, the offline strategy inherently separated the control and update periods, resulting in simultaneous real-time learning being impractical for control. Thus, a potentially optimal hybrid strategy could involve initial offline training in simulations, followed by online fine-tuning to bridge the simulation-to-real performance gap. Within such a hybrid scheme, slow system-inherent variations and typical external condition changes can be handled by occasional light fine-tuning with newly collected data. In contrast, major hardware or configuration modifications would reasonably require a full offline retraining of the compensator.

After establishing the advantages of offline training, the performance of the proposed offline-trained G-PID controller was evaluated using three distinct multi-DoF fusions. Among these, unified DoF modularization consistently provided the most effective compensation. This superiority could be attributed to the integrated representation of inter-DoF coupling, which effectively captured mutual interactions from the outset.

Conversely, batch-separated DoF conditioning, previously employed in [16], maintained DoF distinctions by labeling and separating batch inputs. Although computationally efficient and capable of addressing moderate coupling, this approach often restricted the inter-DoF information flow, limiting its ability to accurately model strong coupling interactions. Independent DoF modularization treated each DoF individually with separate networks, thereby accurately modeling individual DoF characteristics while neglecting mutual coupling and reducing the overall effectiveness in strongly coupled scenarios.

Despite its clear advantages, unified DoF modularization increased the computational complexity as the number of DoFs increased, demanding higher computational resources. Batch-separated conditioning could prove advantageous in scenarios characterized by distinct DoF dynamics or moderate coupling owing to reduced computational demands. Similarly, independent modularization may be preferable when the DoFs exhibit minimal interactions and strong independence.

The evident performance gap between the online and offline-trained G-PID controllers could be attributed to computational and algorithmic limitations inherent in the online learning framework. In particular, online-trained G-PID requires gradient-based updates at every time step, introducing considerable computational overhead that can hinder real-time applicability in control loops. Moreover, soft robotic systems—particularly those with multi-DoF—are characterized by strong nonlinearities and inter-joint coupling, which can cause substantial fluctuations in the learning gradient over time. As online-trained G-PID relies on single-step updates, it is highly sensitive to abrupt gradient variations, often resulting in instability or suboptimal control performance.

In summary, although the strategies all eventually achieved acceptable control performance with extended training, unified DoF modularization demonstrated the fastest convergence and highest accuracy. Given these outcomes, employing an offline-trained G-PID controller in conjunction with unified DoF modularization is recommended, particularly for strongly coupled multi-DoF soft robots, where rapid convergence and high control accuracy are essential.

B. Offline-Trained G-PID Controller in Prototype Experiment

Given that the adaptive controller was trained solely on the 5.4 mm endoscope but tested on considerably different instruments, the experimental results demonstrated that the generator compensator successfully inferred and neutralized instrument-specific disturbances that were absent from the training dataset. This highlights the ability of the controller to adaptively manage disturbances based on learned residual dynamics rather than merely fitting to specific training geometries. Moreover, the simultaneous low errors evident across both DoFs confirmed that the unified fusion strategy could effectively handle the inter-chamber coupling dynamics. Notably, no drift or cross-axis interference occurred, confirming robust adaptive compensation under real-time multi-DoF conditions.

The settling time of approximately 6–7 s, which was longer than the typical 0.2–3 s reported for gripper-type soft actuators, can be attributed primarily to deliberate geometric constraints rather than control performance limitations. In particular, the actuator maintained a relatively large 7 mm internal working channel designed to accommodate diverse surgical instruments. This design reduced the available chamber volume and decreased the internal volume-to-orifice ratio of the chambers. Consequently, the pneumatic time constant increased, necessitating higher absolute pressures (up to 100 kPa) to achieve a substantial tip curvature. During initial inflation, the thin chamber walls preferentially expanded inward into the central channel before outward bending occurred, further delaying effective curvature formation. Collectively, these geometric constraints produced a slow, first-order-like dynamic response, intensifying inter-chamber coupling and highlighting the limitations of conventional PID control ($\pm$1.5 mm errors). By contrast, the proposed offline-trained G-PID controller consistently maintained errors below $\pm$0.9 mm, demonstrating its superior performance even under challenging dynamic conditions.

Although slow actuator responses limited high-speed performance, this constraint arose from the geometric and pneumatic design rather than control limitations and is thus addressable. Engineering solutions include optimizing the geometry to balance the working channel size and chamber volume, tailoring the wall structure and materials, and employing high-flow valves to reduce pneumatic delays. Control strategies such as bounded-angle PID can further mitigate slow dynamics. Notably, the proposed offline-trained G-PID maintained tip errors below $\pm$0.9 mm under current constraints, indicating that targeted hardware–control co-design could reduce response times without compromising accuracy.

C. Limitations and Future Work

Despite these promising results, this study presents some limitations that warrant further investigation. First, the experimental validation was limited to planar bending tasks, leaving

IEEE Transactions on Automation Science and Engineering (T-ASE) paper, presented at ICRA 2026, Vienna, Austria.

the robustness of the controller in more complex 3D maneuvers and prolonged surgical procedures with varying payloads unverified. In addition, as the number of DoFs increases, the computational burden introduced by the unified DoF fusion framework may hinder real-time control, thereby highlighting scalability concerns. Second, although the offline-trained G-PID controller demonstrated improved adaptability, it currently lacks formal stability guarantees and requires manual gain retuning during sim-to-real transfer. These limitations restrict its robustness and responsiveness to intraoperative variations in clinical scenarios. Moreover, neither a purely offline nor online scheme is universally optimal; a practical balance can be achieved, for example, by relying on the offline-trained compensator under nominal tracking errors and gradually increasing the contribution of an online adaptive module only when persistent error growth or abrupt disturbances are detected. Finally, the 6–7 s settling time, although acceptable for low-bandwidth surgical tasks (e.g., prostate probing and laser ablation), is suboptimal for tasks requiring higher dynamic responsiveness, primarily owing to the geometric constraints from the narrow chamber design and the resultant high pneumatic time constant.

Future work should address these limitations as follows:

1) Comprehensive experiments should encompass full-range 3D surgical maneuvers and realistic surgical payload scenarios.
2) Network compression methods (e.g., pruning and knowledge distillation) should be applied to enhance the real-time performance of higher-DoF robots.
3) Rigorous stability proofs and automated adaptive tuning mechanisms (such as meta-learning or Bayesian optimization) should be developed to improve intraoperative adaptability and robustness.
4) Hardware optimization involving increased chamber width and the integration of dual-line high-flow valves should be conducted.

Preliminary finite element and CFD simulations predict that these hardware refinements could reduce the pneumatic time constant by $\geq$ 70%, targeting $<$ 2 s (90% settling) while preserving the required 7 mm working channel. Together, these advances could ensure the safe, reliable, and clinically relevant deployment of adaptive soft robotic controllers.

VI. Conclusion

In this study, an offline-trained GAN-augmented adaptive control strategy (offline-trained G-PID) was tailored for multi-DoF pneumatic soft surgical robots. Among the three evaluated multi-DoF fusion strategies, the unified DoF modularization strategy most effectively captured inter-chamber coupling, consistently delivering submillimeter accuracy ($< \pm 0.9$ mm) in tip position control across diverse clinical endoscopes. Prototype validations confirmed robust generalization to instruments that were markedly different from the training configurations, highlighting their enormous clinical potential. The proposed GAN-based adaptive approach effectively addressed nonlinearities and coupling dynamics, enabling real-time compensation without explicit physical modeling. Future research should focus on validating controller performance during prolonged and complex surgical maneuvers, optimizing computational scalability through network compression techniques, and integrating formal stability proofs alongside automated adaptive tuning to enhance clinical reliability. Overall, the proposed offline-trained GAN-augmented adaptive control approach provides a promising pathway for safer and more precise pneumatic soft robots in minimally invasive surgeries and broader mechatronic systems with nonlinear and coupled dynamics.

Acknowledgment

The authors thank Tianyi Yang for their assistance in the experimentation and figure preparation processes. They also thank Beijing NOKOV Science and Technology Company Ltd., for supporting this study and Editage (www.editage.cn) for the English language editing.

Appendix

See (Table VI, Table VII, and Table VIII)

References

[1] D. Rus and M. T. Tolley, "Design, fabrication and control of soft robots," *Nature*, vol. 521, no. 7553, pp. 467–475, May 2015, doi: 10.1038/nature14543.

[2] C. Laschi, B. Mazzolai, and M. Cianchetti, "Soft robotics: Technologies and systems pushing the boundaries of robot abilities," *Sci. Robot.*, vol. 1, no. 1, pp. 1–11, Dec. 2016, doi: 10.1126/scirobotics.aah3690.

[3] J. Guo, J.-H. Low, X. Liang, J. S. Lee, Y.-R. Wong, and R. C. H. Yeow, "A hybrid soft robotic surgical gripper system for delicate nerve manipulation in digital nerve repair surgery," *IEEE/ASME Trans. Mechatronics*, vol. 24, no. 4, pp. 1440–1451, Aug. 2019, doi: 10.1109/TMECH.2019.2924518.

[4] G. Fang et al., "Soft robotic manipulator for intraoperative MRI-guided transoral laser microsurgery," *Sci. Robot.*, vol. 6, no. 57, pp. 1–13, Aug. 2021, doi: 10.1126/scirobotics.abg5575.

[5] I. De Falco, M. Cianchetti, and A. Menciassi, "A soft multi-module manipulator with variable stiffness for minimally invasive surgery," *Bioinspiration Biomimetics*, vol. 12, no. 5, Sep. 2017, Art. no. 056008, doi: 10.1088/1748-3190/aa7ccd.

[6] A. Giri, C. Girerd, J. Cervera-Torralba, M. T. Tolley, and T. K. Morimoto, "InchIGRAB: An inchworm-inspired guided retraction and bending device for vine robots during colonoscopy," *IEEE/ASME Trans. Mechatronics*, early access, Mar. 5, 2025, doi: 10.1109/TMECH.2025.3535876.

[7] Y. Li, Y. Liu, K. Yamazaki, M. Bai, and Y. Chen, "Development of a soft robot based photodynamic therapy for pancreatic cancer," *IEEE/ASME Trans. Mechatronics*, vol. 26, no. 6, pp. 2977–2985, Dec. 2021, doi: 10.1109/TMECH.2021.3049354.

[8] F. Connolly, C. J. Walsh, and K. Bertoldi, "Automatic design of fiber-reinforced soft actuators for trajectory matching," *Proc. Nat. Acad. Sci. USA*, vol. 114, no. 1, pp. 51–56, Jan. 2017, doi: 10.1073/pnas.1615140114.

[9] M. McCandless, A. Gerald, A. Carroll, H. Aihara, and S. Russo, "A soft robotic sleeve for safer colonoscopy procedures," *IEEE Robot. Autom. Lett.*, vol. 6, no. 3, pp. 5292–5299, Jul. 2021, doi: 10.1109/LRA.2021.3073651.

[10] V. Vikas, P. Grover, and B. Trimmer, "Model-free control framework for multi-limb soft robots," in *Proc. IEEE/RSJ Int. Conf. Intell. Robots Syst. (IROS)*, Hamburg, Germany, Sep. 2015, pp. 1111–1116, doi: 10.1109/IROS.2015.7353509.

[11] J. Yang, E. Harsono, and H. Yu, "Dynamics-based motion control for a hybrid-driven continuum robot with continuously variable stiffness," *IEEE Trans. Autom. Sci. Eng.*, vol. 22, pp. 9049–9060, 2025, doi: 10.1109/TASE.2024.3496773.

[12] H. Wang, X. Wang, W. Yang, Z. Du, and Z. Yan, "Construction of controller model of notch continuum manipulator for laryngeal surgery based on hybrid method," *IEEE/ASME Trans. Mechatronics*, vol. 26, no. 2, pp. 1022–1032, Apr. 2021, doi: 10.1109/TMECH.2020.3015133.

IEEE Transactions on Automation Science and Engineering (T-ASE) paper, presented at ICRA 2026, Vienna, Austria.

[13] Y. Wang, H. Wang, Z. Liu, and W. Chen, "Visual servo-collision avoidance hybrid task by considering detection and localization of contact for a soft manipulator," *IEEE/ASME Trans. Mechatronics*, vol. 25, no. 3, pp. 1310–1321, Jun. 2020, doi: 10.1109/TMECH.2020.2974296.

[14] A. Shu, B. Deutschmann, A. Dietrich, C. Ott, and A. Albu-Schäffer, "Robust H∞ control of a tendon–driven elastic continuum mechanism via a systematic description of nonlinearities," *IFAC-PapersOnLine*, vol. 51, no. 22, pp. 386–392, 2018, doi: 10.1016/j.ifacol.2018.11.572.

[15] A. Abu Alqumsan, S. Khoo, and M. Norton, "Multi-surface sliding mode control of continuum robots with mismatched uncertainties," *Meccanica*, vol. 54, no. 14, pp. 2307–2316, Nov. 2019, doi: 10.1007/s11012-019-01072-6.

[16] A. Hosseini and T. Taghikhany, "Online self-tuning mechanism for direct adaptive control of tall building," *Int. J. Adapt. Control Signal Process.*, vol. 32, no. 3, pp. 424–446, Mar. 2018, doi: 10.1002/acs.2850.

[17] C. M. Best, M. T. Gillespie, P. Hyatt, L. Rupert, V. Sherrod, and M. D. Killpack, "A new soft robot control method: Using model predictive control for a pneumatically actuated humanoid," *IEEE Robot. Autom. Mag.*, vol. 23, no. 3, pp. 75–84, Sep. 2016, doi: 10.1109/MRA.2016.2580591.

[18] Q. Zhao, S. Wang, J. Hu, H. Liu, and H. K. Chu, "Controller design for a soft continuum robot with concurrent continuous rotation," *IEEE/ASME Trans. Mechatronics*, vol. 29, no. 6, pp. 4504–4513, Dec. 2024, doi: 10.1109/TMECH.2024.3378274.

[19] C. Della Santina et al., "Controlling soft robots: Balancing feedback and feedforward elements," *IEEE Robot. Autom. Mag.*, vol. 24, no. 3, pp. 75–83, Sep. 2017, doi: 10.1109/MRA.2016.2636360.

[20] H. Wang, B. Yang, Y. Liu, W. Chen, X. Liang, and R. Pfeifer, "Visual servoing of soft robot manipulator in constrained environments with an adaptive controller," *IEEE/ASME Trans. Mechatronics*, vol. 22, no. 1, pp. 41–50, Feb. 2017, doi: 10.1109/TMECH.2016.2613410.

[21] J. Lai, K. Huang, B. Lu, Q. Zhao, and H. Chu, "Verticalized-tip trajectory tracking of a 3D-printable soft continuum robot: Enabling surgical blood suction automation," *IEEE/ASME Trans. Mechatronics*, vol. 27, no. 3, pp. 1545–1556, Jun. 2022, doi: 10.1109/TMECH.2021.3090838.

[22] Z. Chen et al., "Data-driven methods applied to soft robot modeling and control: A review," *IEEE Trans. Autom. Sci. Eng.*, vol. 22, pp. 2241–2256, 2025, doi: 10.1109/TASE.2024.3377291.

[23] S. Zhong et al., "Paired interactions of magnetic millirobots in confined spaces through data-driven disturbance rejection control under global input," *IEEE/ASME Trans. Mechatronics*, early access, Jan. 15, 2025, doi: 10.1109/TMECH.2024.3521085.

[24] H. Wang et al., "Data-driven parallel adaptive control for magnetic helical microrobots with derivative structure in uncertain environments," *IEEE Trans. Syst., Man, Cybern., Syst.*, vol. 54, no. 7, pp. 4139–4150, Jul. 2024, doi: 10.1109/TSMC.2024.3374071.

[25] X. Pei, R. Shi, L. Wang, S. Liu, Z. Wu, and Z. Dai, "A programmable pneumatic system with novel improved controller enabling adhesion and desorption operations of soft adhesive robots," *IEEE Trans. Autom. Sci. Eng.*, vol. 22, pp. 19986–19999, 2025, doi: 10.1109/TASE.2025.3599688.

[26] A. Centurelli, L. Arleo, A. Rizzo, S. Tolu, C. Laschi, and E. Falotico, "Closed-loop dynamic control of a soft manipulator using deep reinforcement learning," *IEEE Robot. Autom. Lett.*, vol. 7, no. 2, pp. 4741–4748, Apr. 2022, doi: 10.1109/LRA.2022.3146903.

[27] H. Mo, R. Wei, X. Kong, Y. Zhai, Y. Liu, and D. Sun, "Data-efficient learning control of continuum robots in constrained environments," *IEEE Trans. Autom. Sci. Eng.*, vol. 22, pp. 984–995, 2025, doi: 10.1109/TASE.2024.3357816.

[28] F. Cursi, W. Bai, E. M. Yeatman, and P. Kormushev, "Task accuracy enhancement for a surgical macro-micro manipulator with probabilistic neural networks and uncertainty minimization," *IEEE Trans. Autom. Sci. Eng.*, vol. 21, no. 1, pp. 241–256, Jan. 2024, doi: 10.1109/TASE.2022.3219590.

[29] P. Xiang et al., "Learning-based high-precision force estimation and compliant control for small-scale continuum robot," *IEEE Trans. Autom. Sci. Eng.*, vol. 21, no. 4, pp. 5389–5401, Oct. 2024, doi: 10.1109/TASE.2023.3311179.

[30] Z. Q. Tang, H. L. Heung, K. Y. Tong, and Z. Li, "Model-based online learning and adaptive control for a 'human-wearable soft robot' integrated system," *Int. J. Robot. Res.*, vol. 40, no. 1, pp. 256–276, Jan. 2021, doi: 10.1177/0278364919873379.

[31] Z. Zhou, Y. Lu, S. Kokubu, P. E. Tortós, and W. Yu, "A GAN based PID controller for highly adaptive control of a pneumatic-artificial-muscle driven antagonistic joint," *Complex Intell. Syst.*, vol. 10, no. 5, pp. 6231–6248, Oct. 2024, doi: 10.1007/s40747-024-01488-y.

[32] W. Chen, C. Xiong, C. Liu, P. Li, and Y. Chen, "Fabrication and dynamic modeling of bidirectional bending soft actuator integrated with optical waveguide curvature sensor," *Soft Robot.*, vol. 6, no. 4, pp. 495–506, Aug. 2019, doi: 10.1089/soro.2018.0061.

[33] E. H. Skorina, M. Luo, S. Ozel, F. Chen, W. Tao, and C. D. Onal, "Feedforward augmented sliding mode motion control of antagonistic soft pneumatic actuators," in *Proc. IEEE Int. Conf. Robot. Autom. (ICRA)*, Seattle, WA, USA, May 2015, pp. 2544–2549, doi: 10.1109/ICRA.2015.7139540.

[34] C. D. Onal and D. Rus, "Autonomous undulatory serpentine locomotion utilizing body dynamics of a fluidic soft robot," *Bioinspiration Biomimetics*, vol. 8, no. 2, Mar. 2013, Art. no. 026003, doi: 10.1088/1748-3182/8/2/026003.

[35] D. Vrabie, K. G. Vamvoudakis, and F. L. Lewis, "MRAC revisited: Guaranteed performance with reference model modification," *IEEE Trans. Autom. Control*, vol. 56, no. 6, pp. 1352–1358, Jun. 2011, doi: 10.1109/ACC.2010.5530648.

[36] Y. Lu, Z. Zhou, P. E. Tortos Vinocour, S. Kokubu, T. Igarashi, and W. Yu, "Effects of chamber shapes on maneuverability and control property of endoscope-support soft actuators," *Frontiers Bioeng. Biotechnol.*, vol. 11, pp. 1–17, Dec. 2023, doi: 10.3389/fbioe.2023.1319922.

Yuxi Lu (Member, IEEE) received the Ph.D. degree in medical engineering from the Graduate School of Science and Engineering, Chiba University, Chiba, Japan, in 2024, and the M.S. and B.S. degrees in engineering from Tokyo University of Science, Tokyo, Japan, in 2021 and 2019, respectively. He is currently an Assistant Professor with Shanghai Research Institute for Intelligent Autonomous Systems, Tongji University, Shanghai, China. His current research interests include medical robotics and soft robotic systems, particularly their application in minimally invasive surgeries and rehabilitation.

Zhongchao Zhou received the B.Eng. degree in electromechanical engineering from Qingdao University of Science and Technology, Qingdao, China, in 2018, and the M.Eng. and Ph.D. degrees in medical engineering from Chiba University, Japan, in 2021 and 2024, respectively. In 2023, he was a Visiting Research Scholar at the Healthcare Biorobotics Laboratory, Institute of Biomedical Engineering, University of Oxford, U.K. He is currently a Senior Researcher with the School of Engineering, The University of Tokyo. His research interests include soft robotics, control theory, and learning controls.

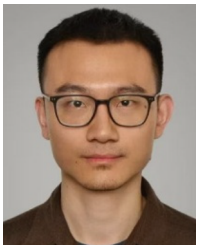

Dongliang Zheng (Member, IEEE) received the B.Eng. degree in automation from Northeastern University, Shenyang, China, in 2015, the M.S. degree in control engineering from Shanghai Jiao Tong University, Shanghai, China, in 2018, and the Ph.D. degree in aerospace engineering from Georgia Institute of Technology, Atlanta, GA, USA, in 2024. He is currently an Assistant Professor with Shanghai Research Institute for Intelligent Autonomous Systems, Tongji University. His research interests include motion planning and control for autonomous robots.

IEEE Transactions on Automation Science and Engineering (T-ASE) paper, presented at ICRA 2026, Vienna, Austria.

Yanmin Zhou (Member, IEEE) received the M.S. degree in control theory and control engineering from Tongji University, Shanghai, China, in 2011, and the Ph.D. degree in biomechanics from the University of Cambridge, Cambridge, U.K., in 2015. She is currently an Associate Professor with the Department of Control Science and Engineering, College of Electronics and Information Engineering, Tongji University. Her current research interests include bionics and the design and control of intelligent robots.

Zhipeng Wang (Member, IEEE) received the M.S. degree in mechanical manufacturing and automation from Zhejiang University, Hangzhou, China, in 2011, and the Ph.D. degree in control science and engineering from Tongji University, Shanghai, China, in 2015. He is currently an Associate Professor with the Department of Control Science and Engineering, Tongji University. His research interests include robot motion planning, mechatronics, and dynamics.

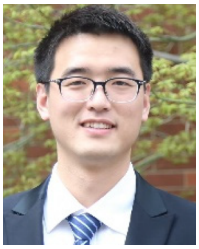

Shuo Jiang (Member, IEEE) received the B.E. degree in mechatronic engineering from Zhejiang University, Hangzhou, China, in 2015, and the Ph.D. degree in mechanical engineering from Shanghai Jiao Tong University, Shanghai, China, in 2020. From September 2019 to September 2020, he was a Visiting Scholar with Imperial College London, London, U.K. He is currently an Associate Professor with the Department of Control Science and Engineering, College of Electronics and Information Engineering, Tongji University, Shanghai. His research interests include human–machine interaction, intelligent sensing, and robotics.

Wenwei Yu (Member, IEEE) received the B.Eng. and M.Eng. degrees from Shanghai Jiao Tong University in 1989 and 1992, respectively, and the Ph.D. degrees in system information engineering and rehabilitation medical science from Hokkaido University, Japan, in 1997 and 2003, respectively. He was an Assistant Professor with the Department of System Information Engineering, School of Engineering, Hokkaido University, from 1999 to 2003. In 2003, he was an Exchange Research Fellow with the Center for Neuroscience, University of Alberta, Canada, supported by the Researcher Exchange Program of Japanese Society for the Promotion of Science (JSPS). Since 2004, he has been an Associate Professor with the Department of Medical System Engineering, School of Engineering, Chiba University, Japan. He has been a Professor at Chiba University since 2009. His research interests include neuroprosthetics, rehabilitation robotics, motor control, and biomedical signal processing.

Bin He (Senior Member, IEEE) received the Ph.D. degree in mechanical and electronic control engineering from Zhejiang University, Hangzhou, China, in 2001. From 2001 to 2003, he held post-doctoral research appointments with the State Key Laboratory of Fluid Power Transmission and Control, Zhejiang University. He is currently a Professor with the College of Electronics and Information Engineering, Tongji University, Shanghai, China. His current research interests include intelligent robotic control, biomimetic microrobots, and wireless networks.